

A general theory that can accurately predict the relationship between the tractive effort and the longitudinal slip of pneumatic tires on hard surfaces has yet to be evolved. However, several theories have been proposed that could provide a basic understanding of the physical nature of the processes involved. One of the earliest theoretical treatises on the relationship between the tractive effort and the longitudinal slip of pneumatic tires was presented by Julien [1.15].

In Julien's theory, it is assumed that the tire tread can be regarded as an elastic band, and that the contact patch is rectangular and the normal pressure is uniformly distributed [1.15]. It is further assumed that the contact patch can be divided into an adhesion region and a sliding region. In the adhesion region, the interacting forces depend on the elastic properties of the tire, whereas in the sliding region, the interacting forces depend upon the adhesive properties of the tire-ground interface. When a driving torque is applied to a tire, in the region in front of the contact patch, the driving torque produces a longitudinal strain ϵ (in compression) in the tread. It remains constant in the adhesion region of the contact patch, where no sliding between the tire tread and the ground takes place. Let e_0 be the longitudinal deformation of the tire tread in front of the contact patch, and let e be the longitudinal deformation of the tread at a point at a distance x behind the front contact point

$$e = e_0 + x\epsilon \quad (1.7)$$

Assume that e_0 is proportional to ϵ , and $e_0 = \lambda\epsilon$. Then

$$e = (\lambda + x)\epsilon \quad (1.8)$$

It is further assumed that, within the adhesion region, where no sliding between the tire tread and the ground takes place, the tractive force per unit contact length is proportional to the deformation of the tread. Thus,

$$\frac{dF_x}{dx} = k_t e = k_t(\lambda + x)\epsilon \quad (1.9)$$

where k_t is the tangential stiffness of the tire tread and F_x is the tractive force. Based on experimental data of a sample of heavy truck tires under rated loads and inflation pressures, it is found that the value of k_t varies in a narrow range from approximately 3930 kN/m² (570 lb/in.²) for a radial-ply tire to 4206 kN/m² (610 lb/in.²) for a bias-ply tire.

$$F_x = \int_0^x k_t(\lambda + x)\epsilon dx = k_t\lambda x\epsilon \left(1 + \frac{x}{2\lambda}\right) \quad (1.10)$$

Let p be the normal pressure, b the width of the contact patch, and μ_p the

peak value of the coefficient of road adhesion. Then no sliding will take place between the tread and the ground if the following condition is satisfied:

$$\frac{dF_x}{dx} = k_t(\lambda + x)\epsilon \leq \mu_p pb \quad (1.11)$$

This implies that if a point at a distance of x behind the front contact point is in the adhesion region, then x must be less than a characteristic length l_c , which defines the length of the region where no sliding between the tire tread and the ground takes place, that is,

$$x \leq l_c = \frac{\mu_p pb}{k_t \epsilon} - \lambda = \frac{\mu_p W}{l_t k_t \epsilon} - \lambda \quad (1.12)$$

where W is the normal load on the tire and l_t is the contact length of the tire.

If $l_t \leq l_c$, then the entire contact area is an adhesion region. Letting $x = l_t$ in Eq. 1.10, the tractive force becomes

$$F_x = k_t \lambda l_t \epsilon \left(1 + \frac{l_t}{2\lambda} \right) = K_t \epsilon \quad (1.13)$$

where $K_t = k_t \lambda l_t [1 + l_t/2\lambda]$.

Since the longitudinal strain ϵ is a measure of the longitudinal slip i of the tire, it is concluded that if the entire contact patch is an adhesion region, the relationship between the tractive force F_x and the slip i is linear. This corresponds to the region between points O and A on the tractive effort–slip curve shown in Fig. 1.16.

The condition for sliding at the rear edge of the contact area is given by

$$l_t = l_c = \frac{\mu_p W}{l_t k_t i} - \lambda \quad (1.14)$$

This means that, if the slip or tractive force reaches the respective critical value i_c or F_{xc} given below, sliding in the trailing part of the contact patch begins:

$$i_c = \frac{\mu_p W}{l_t k_t (l_t + \lambda)} \quad (1.15)$$

$$F_{xc} = \frac{\mu_p W [1 + (l_t/2\lambda)]}{1 + (l_t/\lambda)} \quad (1.16)$$

A further increase of slip or tractive force beyond the respective critical

value results in the spread of the sliding region from the trailing edge towards the leading part of the contact patch. The tractive force F_{xs} developed in the sliding region is given by

$$F_{xs} = \mu_p W (1 - l_c/l_t) \quad (1.17)$$

and the tractive force F_{xa} developed in the adhesion region is given by

$$F_{xa} = k_t \lambda i l_c \left(1 + \frac{l_c}{2\lambda} \right) \quad (1.18)$$

where l_c is determined by Eq. 1.12.

Hence, the relationship between the total tractive force and the slip when part of the tire tread sliding on the ground is expressed by

$$F_x = F_{xs} + F_{xa} = \mu_p W - \frac{\lambda(\mu_p W - K' i)^2}{2l_t K' i} \quad (1.19)$$

where $K' = l_t k_t \lambda$.

This equation clearly indicates the nonlinear behavior of the tractive effort–longitudinal slip relationship when sliding occurs in part of the contact area. This corresponds to the region beyond point *A* of the curve shown in Fig. 1.16.

When sliding extends over the entire contact patch, the tractive force F_x is equal to $\mu_p W$. Under this condition, the slip i is obtained by setting l_c to zero in Eq. 1.14. The value of the slip i_m where the maximum tractive effort occurs is equal to $\mu_p W / l_t k_t \lambda$ and corresponds to point *B* shown in Fig. 1.16. A further increase of tire slip results in an unstable situation, with the coefficient of road adhesion falling rapidly from the peak value μ_p to the pure sliding value μ_s .

In practice, the normal pressure distribution over the tire–ground contact patch is not uniform. There is a gradual drop of pressure near the edges. It is expected, therefore, that a small sliding region will be developed in the trailing part of the contact area, even at low slips.

Using Julien's theory to define the relationship between tractive effort and longitudinal slip, in addition to the parameters μ_p , W , and l_t , the value of λ , which determines the longitudinal deformation of the tire tread prior to entering the contact patch, must be known. To determine the value of λ for a given tire would require considerable effort and elaborate experiments. In view of this, a simplified theory has been developed in which the effect of λ is neglected. From Eq. 1.9, by neglecting the term λ , the tractive force per unit contact length in the adhesion region at a distance of x from the front contact point is given by

$$\frac{dF_x}{dx} = k_t x \epsilon = k_t x i \quad (1.20)$$

If there is no sliding between the tire tread and the ground for the entire contact patch, the relationship between the tractive force and slip can be expressed by

$$F_x = \int_0^{l_t} k_t i x \, dx = (k_t l_t^2 / 2) i \quad (1.21)$$

The term $k_t l_t^2 / 2$ may be taken as the slope C_i of the tractive effort–slip curve at the origin as shown in Fig. 1.16, that is,

$$\frac{k_t l_t^2}{2} = C_i = \tan \theta = \left. \frac{\partial F_x}{\partial i} \right|_{i=0} \quad (1.22)$$

where C_i is usually referred to as the longitudinal stiffness of the tire.

If no sliding takes place on the contact patch, the relationship between the tractive force and the slip will, therefore, be linear:

$$F_x = C_i i \quad (1.23)$$

Equation 1.23 applies to section OA of the curve shown in Fig. 1.16.

With the increase of slip beyond point A shown in Fig. 1.16, the tractive force per unit contact length at the trailing edge of the contact patch reaches the adhesion limit, and sliding between the tread and the ground takes place.

$$\frac{dF_x}{dx} = k_t l_t i = \mu_p p b = \frac{\mu_p W}{l_t} \quad (1.24)$$

This indicates that when the slip or tractive force reaches the respective critical value i_c or F_{xc} given below, sliding in the trailing part of the contact patch begins:

$$i_c = \frac{\mu_p W}{k_t l_t^2} = \frac{\mu_p W}{2C_i} \quad (1.25)$$

$$F_{xc} = C_i i_c = \frac{\mu_p W}{2} \quad (1.26)$$

In other words, if slip $i \leq i_c$ or the tractive force $F_x \leq F_{xc}$, the relationship between the tractive force and slip is linear, as shown in Fig. 1.16. Equation 1.26 indicates that the upper limit for the linear range of the tractive force–

slip relationship is identified by the tractive force being equal to one half of its maximum value ($\mu_p W/2$).

A further increase of slip or tractive force beyond the respective critical value (i.e., $i > i_c$ or $F_x > F_{xc}$) results in the spread of the sliding region from the trailing edge towards the leading part of the contact patch. The tractive force F_{xs} developed in the sliding region is given by

$$F_{xs} = \mu_p W \left(1 - \frac{l_c}{l_t} \right) = \mu_p W \left(1 - \frac{\mu_p W}{2C_i i} \right) \quad (1.27)$$

and the tractive force F_{xa} developed in the adhesion region is expressed by

$$F_{xa} = \frac{1}{2} \frac{\mu_p W l_c}{l_t} = \frac{\mu_p^2 W^2}{4C_i i} \quad (1.28)$$

Hence, the relationship between the total tractive force and the slip when part of the tread is sliding on the ground (i.e., $i > i_c$ or $F_x > F_{xc}$) is given by

$$F_x = F_{xs} + F_{xa} = \mu_p W \left(1 - \frac{\mu_p W}{4C_i i} \right) \quad (1.29)$$

The equation above indicates the nonlinear nature of the tractive effort–longitudinal slip relationship when sliding occurs in part of the contact patch. It is applicable to predicting the tractive effort–slip relation when the tractive effort is lower than its maximum value $\mu_p W$.

In comparison with Julien's theory, the simplified theory described above requires only three parameters, μ_p , W , and C_i , to define the tractive effort–longitudinal slip relationship. As pointed out previously, the value of C_i can easily be identified from the initial slope of the measured tractive effort–slip curve.

When a braking torque is applied to the tire, a stretching of the tread elements occurs prior to entering the contact area, as shown in Fig. 1.17, in contrast with the compression effect for a driven tire. The distance that the tire travels when a braking torque is applied, therefore, will be greater than that in free rolling. The severity of braking is often measured by the skid of the tire i_s , which is defined as

$$\begin{aligned} i_s &= \left(1 - \frac{r\omega}{V} \right) \times 100\% \\ &= \left(1 - \frac{r}{r_e} \right) \times 100\% \end{aligned} \quad (1.30)$$

For a locked wheel, the angular speed ω of the tire is zero, whereas the

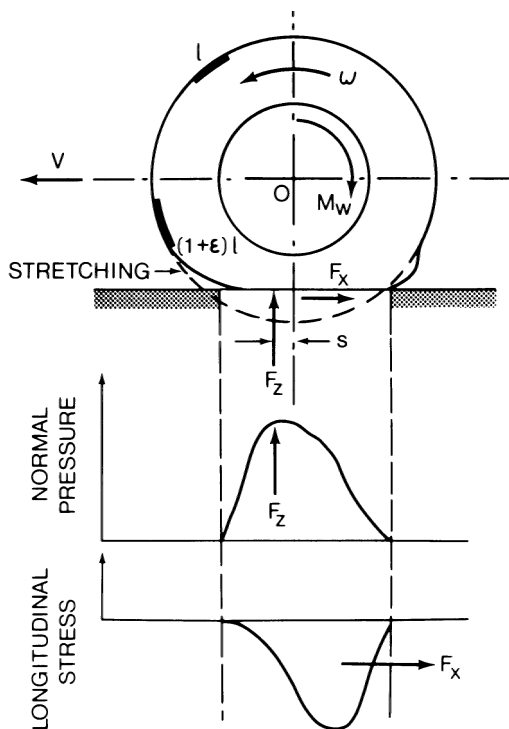


Fig. 1.17 Behavior of a tire under the action of a braking torque. (Reproduced with permission from *Mechanics of Pneumatic Tires*, edited by S.K. Clark, Monograph 122, National Bureau of Standards, 1971.)

linear speed of the tire center is not zero. Under this condition, the skid is denoted 100%. It should be noted that using the definition of slip suggested by the SAE and given by Eq. 1.6, for a locked tire, the slip will be -100% .

A simplified theory for the relationship between the braking effort and the skid can also be developed, following an approach similar to that for the relationship between the tractive force and the slip described previously. It should be mentioned that according to the definitions of slip i and skid i_s given by Eqs. 1.5 and 1.30, respectively, the expressions for slip i and skid i_s are related by

$$|i| = |i_s / (1 - i_s)| \quad (1.31)$$

If no sliding takes place on the contact patch, the relationship between the braking effort and the skid can be established by replacing C_i and i in Eq. 1.23 with C_s and $i_s / (1 - i_s)$, respectively.

$$F_x = C_s i_s / (1 - i_s) \quad (1.32)$$

where F_x is the braking effort acting in the opposite direction of motion of the tire center, and C_s is the slope of the braking effort–skid curve at the origin, and is given by [1.8]

$$C_s = \left. \frac{\partial F_x}{\partial i_s} \right|_{i_s=0} \quad (1.33)$$

C_s is referred to as the longitudinal stiffness of the tire during braking. Similar to the parameter C_i , the value of C_s can easily be identified from the initial slope of the measured braking effort–skid curve.

It is interesting to note from Eq. 1.32 that, using the definition of skid given by Eq. 1.30, the relationship between braking effort and skid is nonlinear, even at low skids, where no sliding takes place between the tread and the ground.

The critical value of skid i_{sc} , at which sliding between the tread and the ground begins, can be established by replacing C_i and i in Eq. 1.25 with C_s and $i_s/(1 - i_s)$, respectively.

$$i_{sc} = \frac{\mu_p W}{2C_s + \mu_p W} \quad (1.34)$$

The corresponding critical value of braking effort F_{xc} , above which sliding between the tread and the ground begins, is given by

$$F_{xc} = \frac{C_s i_{sc}}{1 - i_{sc}} = \frac{\mu_p W}{2} \quad (1.35)$$

When sliding takes place in part of the contact patch (i.e., $i_s > i_{sc}$), the relationship between the braking effort and the skid can be established by replacing C_i and i in Eq. 1.29 with C_s and $i_s/(1 - i_s)$, respectively.

$$F_x = \mu_p W \left[1 - \frac{\mu_p W (1 - i_s)}{4C_s i_s} \right] \quad (1.36)$$

While the theory described above represents a simplified model for the highly complex phenomenon of tire–ground interaction, it has been proven to be useful in representing tire behavior in the simulations of the dynamics of passenger cars [1.8, 1.16].

Figure 1.18 shows the variation of the braking effort coefficient, which is the ratio of the braking effort to the normal load, with skid for a bias-ply passenger car tire over various surfaces [1.17]. The peak and sliding values

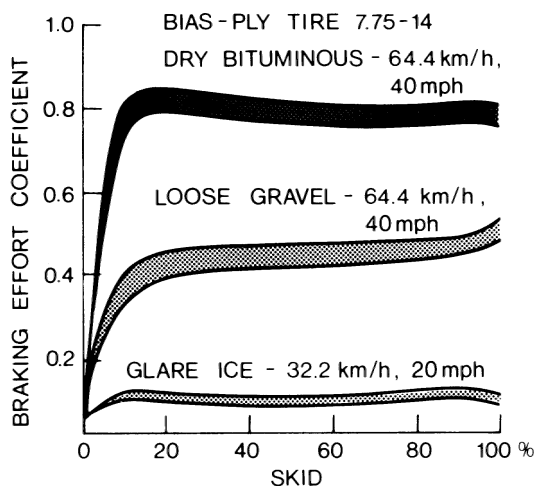


Fig. 1.18 Variation of braking effort coefficient with skid of a car tire on various surfaces. (Reproduced with permission of the Society of Automotive Engineers from reference 1.17.)

of the coefficient of road adhesion of a bias-ply, a bias-belted, and a radial-ply passenger car tire of the same size with various inflation pressures at a speed of 64 km/h (40 mph) on a dry, aggregate asphalt surface are shown in Fig. 1.19 [1.11]. It appears that on a dry surface, the coefficient of road adhesion does not vary significantly with tire construction and inflation pressure. Average peak and sliding values of the coefficient of road adhesion μ_p and μ_s on various surfaces are given in Table 1.2 [1.12].

Among the operational parameters, speed and normal load have noticeable effects on the tractive (braking) effort–slip (skid) characteristics. Figure 1.20 shows the influence of speed on the braking effort coefficient–skid characteristics of a bias-ply truck tire on a dry asphalt surface [1.18]. As shown in Fig. 1.20, speed appears to have a significant effect on the tractive (braking) performance of a tire. Therefore, it has been suggested that to improve the prediction of the relationship between the tractive (braking) effort and the slip (skid), the effect of the sliding speed between the tire tread and the ground should be incorporated into the theories described previously [1.8]. Figure 1.21 shows the effect of normal load on the braking performance of a bias-ply truck tire on a dry asphalt surface [1.18]. It is noted that the value of the longitudinal stiffness C_s increases noticeably with an increase of the normal load. This is because the tire contact length increases with the normal load for a given inflation pressure. According to Eq. 1.21, to develop a given longitudinal force, the longer tire contact length results in lower longitudinal slip (or skid).

A sample of the peak and sliding values of the coefficient of road adhesion μ_p and μ_s for truck tires at 64 km/h (40 mph) on dry and wet concrete

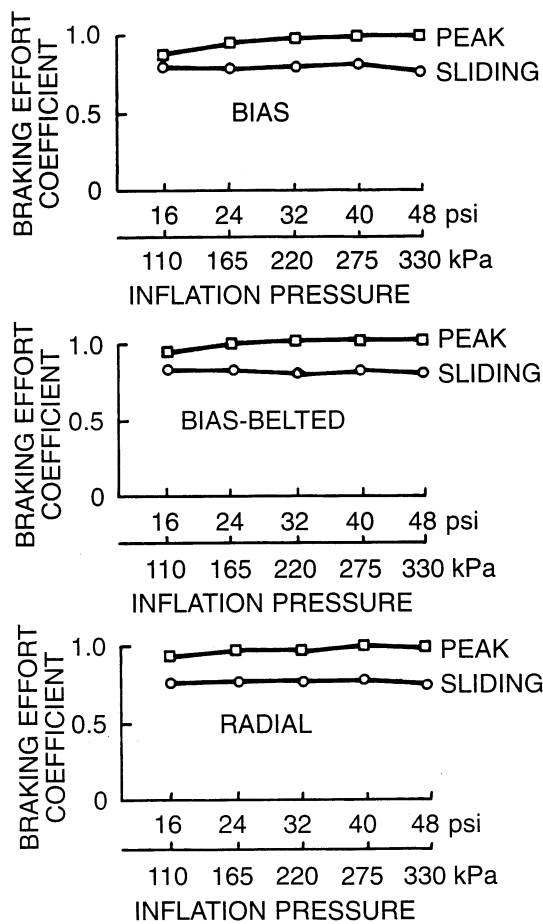


Fig. 1.19 Variation of peak and sliding values of braking effort coefficient with inflation pressure for bias-ply, bias-belted, and radial-ply car tires on dry pavement. (Reproduced with permission of the Society of Automotive Engineers from reference 1.11.)

TABLE 1.2 Average Values of Coefficient of Road Adhesion

Surface	Peak Value μ_p	Sliding Value μ_s
Asphalt and concrete (dry)	0.8–0.9	0.75
Asphalt (wet)	0.5–0.7	0.45–0.6
Concrete (wet)	0.8	0.7
Gravel	0.6	0.55
Earth road (dry)	0.68	0.65
Earth road (wet)	0.55	0.4–0.5
Snow (hard-packed)	0.2	0.15
Ice	0.1	0.07

Source: Reference 1.12.

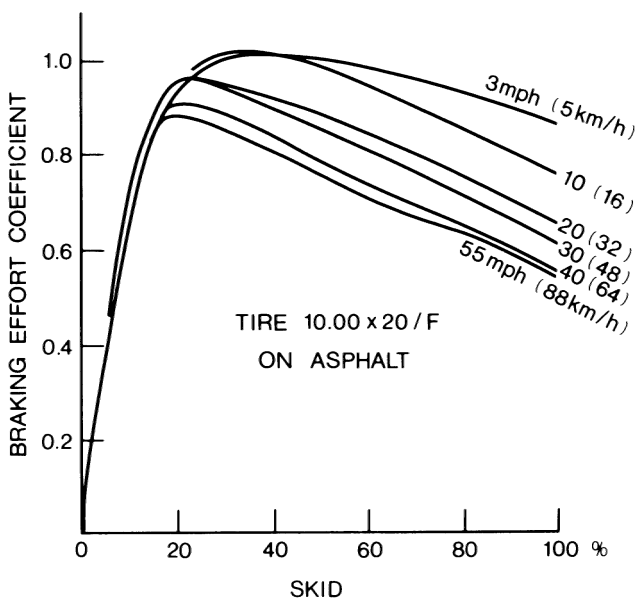


Fig. 1.20 Effect of speed on braking performance of a truck tire on asphalt. (Reproduced with permission from reference 1.18.)

pavements is shown in Table 1.3 [1.19]. The pavements were aggressively textured, like those of relatively new roads meeting the requirements of the U.S. Federal Interstate Highway System.

It can be seen from Table 1.3 that the ratio of the peak value μ_p to the sliding value μ_s for truck tires on dry concrete pavement is around 1.4, whereas on wet concrete pavement, it ranges from approximately 1.3 to 1.6. It is also noted that there appear to be no clear distinctions between the tractive (braking) performance of bias-ply and radial-ply truck tires.

The significant difference between the peak values μ_p and the sliding value μ_s of the coefficient of road adhesion indicates the importance of avoiding wheel lock-up during braking (skid $i_s = 100\%$) or wheel spinning during acceleration (slip $i = 100\%$). This is one of the impetuses to the development of antilock brake systems and traction control systems for road vehicles, which will be discussed in Chapter 3.

1.4 CORNERING PROPERTIES OF TIRES

1.4.1 Slip Angle and Cornering Force

When a pneumatic tire is not subject to any force perpendicular to the wheel plane (i.e., side force), it will move along the wheel plane. If, however, a side

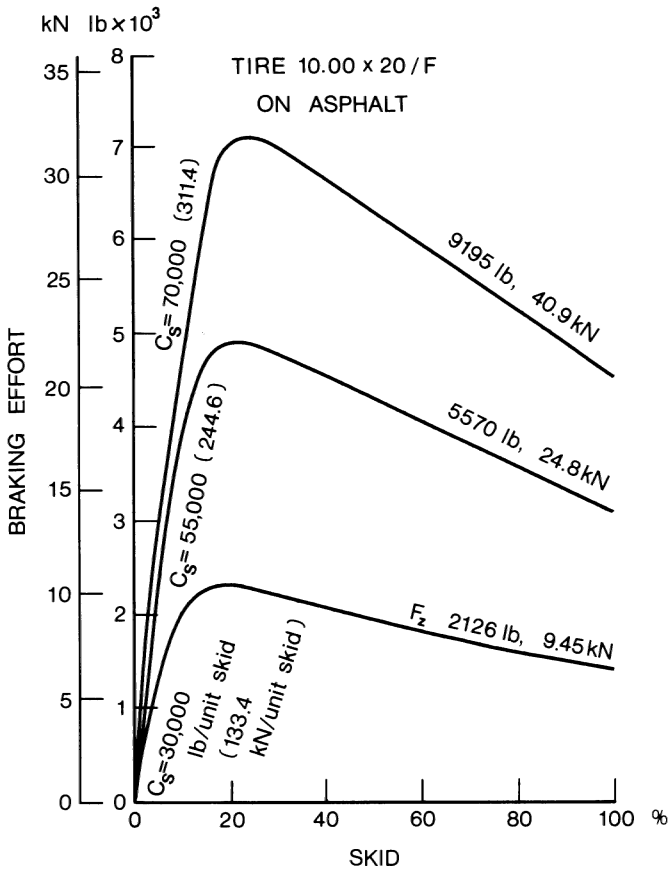


Fig. 1.21 Effect of normal load on braking performance of a truck tire on asphalt. (Reproduced with permission from reference 1.18.)

force F_s is applied to a tire, a lateral force will be developed at the contact patch, and the tire will move along a path at an angle α with the wheel plane, as OA shown in Fig. 1.22. The angle α is usually referred to as the slip angle, and the phenomenon of side slip is mainly due to the lateral elasticity of the tire.

The lateral force developed at the tire-ground contact patch is usually called the cornering force $F_{y\alpha}$ when the camber angle of the wheel is zero. The relationship between the cornering force and the slip angle is of fundamental importance to the directional control and stability of road vehicles.

When the tire is moving at a uniform speed in the direction of OA , the side force F_s applied at the wheel center and the cornering force $F_{y\alpha}$ developed in the ground plane are usually not collinear, as shown in Fig. 1.22. At small slip angles, the cornering force in the ground plane is normally behind the

TABLE 1.3 Values of Coefficient of Road Adhesion for Truck Tires on Dry and Wet Concrete Pavement at 64 km/h (40 mph)

Tire Type	Tire Construction	Dry		Wet	
		μ_p	μ_s	μ_p	μ_s
Goodyear Super Hi Miler (Rib)	Bias-ply	0.850	0.596	0.673	0.458
General GTX (Rib)	Bias-ply	0.826	0.517	0.745	0.530
Firestone Transteel (Rib)	Radial-ply	0.809	0.536	0.655	0.477
Firestone Transport 1 (Rib)	Bias-ply	0.804	0.557	0.825	0.579
Goodyear Unisteel R-1 (Rib)	Radial-ply	0.802	0.506	0.700	0.445
Firestone Transteel Traction (Lug)	Radial-ply	0.800	0.545	0.600	0.476
Goodyear Unisteel L-1 (Lug)	Radial-ply	0.768	0.555	0.566	0.427
Michelin XZA (Rib)	Radial-ply	0.768	0.524	0.573	0.443
Firestone Transport 200 (Lug)	Bias-ply	0.748	0.538	0.625	0.476
Uniroyal Fleet Master Super Lug	Bias-ply	0.739	0.553	0.513	0.376
Goodyear Custom Cross Rib	Bias-ply	0.716	0.546	0.600	0.455
Michelin XZZ (Rib)	Radial-ply	0.715	0.508	0.614	0.459
Average		0.756	0.540	0.641	0.467

Source: UMTRI, reference 1.19.

applied side force, giving rise to a torque (or couple), which tends to align the wheel plane with the direction of motion. This torque is called the aligning or self-aligning torque, and is one of the primary restoring moments which help the steered tire return to the original position after negotiating a turn. The distance t_p between the side force and the cornering force is called the pneumatic trail, and the product of the cornering force and the pneumatic trail determines the self-aligning torque.

The relationships between the slip angle and the cornering force of various types of tire under a variety of operating conditions have been investigated extensively. Typical plots of the cornering force as a function of the slip angle for a bias-ply and a radial-ply passenger car tire are shown in Fig. 1.23 [1.6]. It can be seen that for slip angles below a certain value, such as 4° shown in Fig. 1.23, the cornering force is approximately proportional to the slip angle. Beyond that, the cornering force increases at a lower rate with an increase of the slip angle, and it reaches a maximum value where the tire begins sliding laterally. For passenger car tires, the maximum cornering force may occur at a slip angle of about 18° , while for racing car tires, the cornering force may peak at approximately 6° . Figure 1.23 shows that the cornering force of a bias-ply tire increases more slowly with an increase of the slip angle than that of a radial-ply tire. These characteristics are considered to be more suited to two-wheeled vehicles, such as motorcycles. A more gradual increase of the cornering force with the slip angle enables the driver to exercise better control over a two-wheeled vehicle. This is one of the reasons why bias-ply tires are used for motorcycles [1.1]. Figure 1.24 shows the variations of the

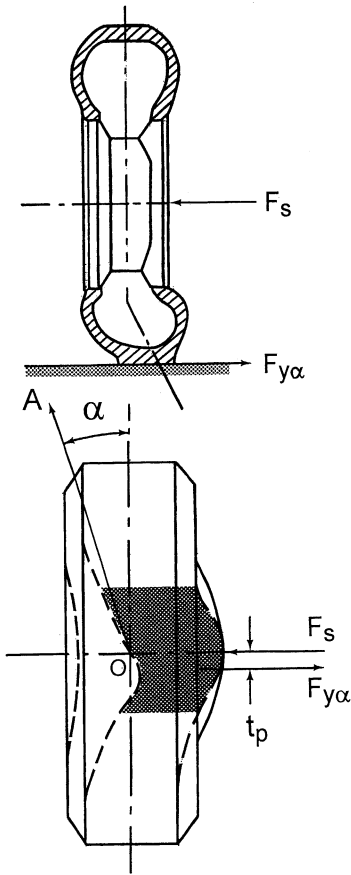


Fig. 1.22 Behavior of a tire subject to a side force. (Reproduced with permission from *Mechanics of Pneumatic Tires*, edited by S.K. Clark, Monograph 122, National Bureau of Standards, 1971.)

ratio of the cornering force to the normal load with the slip angle for radial-ply and bias-ply truck tires of size 10.00–20 with different tread designs (ribbed or lugged) [1.8]. Similar to that shown in Fig. 1.23 for passenger car tires, the cornering force of radial-ply truck tires increases more rapidly with an increase of the slip angle than that of bias-ply truck tires.

A number of factors affect the cornering behavior of pneumatic tires. The normal load on the tire strongly influences the cornering characteristics. Some typical results are shown in Fig. 1.25 [1.6]. It can be seen that for a given slip angle, the cornering force generally increases with an increase of the normal load. However, the relationship between the cornering force and the normal load is nonlinear. Thus, the transfer of load from the inside to the outside tire during a turning maneuver will reduce the total cornering force that a pair of tires can develop. Consider a pair of tires on a beam axle, each with normal load F_z , as shown in Fig. 1.26. The cornering force per tire with normal load F_z is F_y for a given slip angle. If the vehicle undergoes a steady-

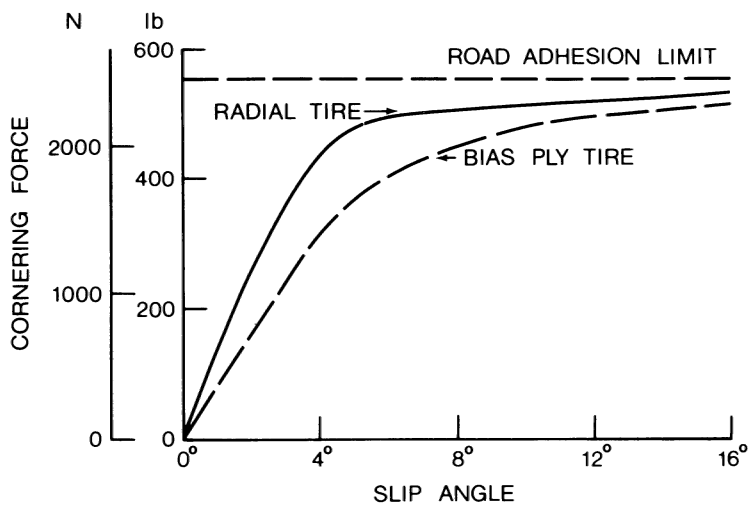


Fig. 1.23 Cornering characteristics of a bias-ply and a radial-ply car tire. (Reproduced with permission from *Mechanics of Pneumatic Tires*, edited by S.K. Clark, Monograph 122, National Bureau of Standards, 1971.)

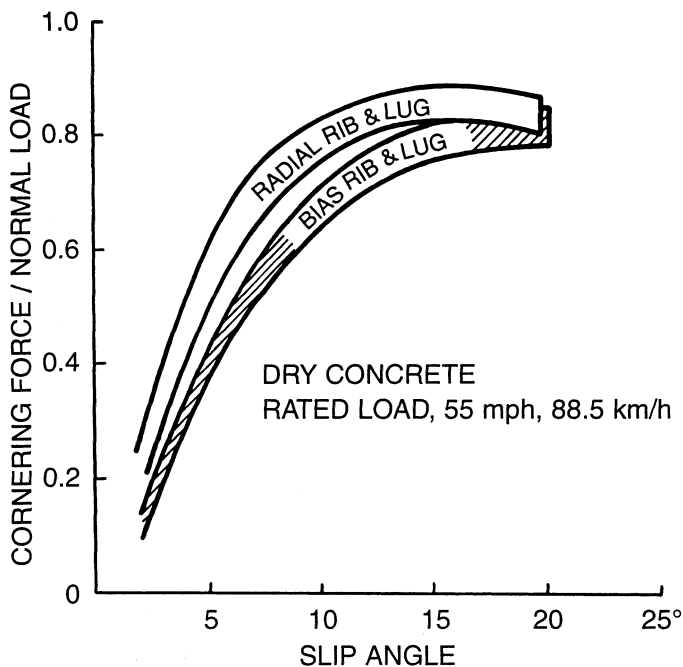


Fig. 1.24 Cornering characteristics of bias-ply and radial-ply truck tires on dry concrete. (Reproduced with permission from reference 1.8.)

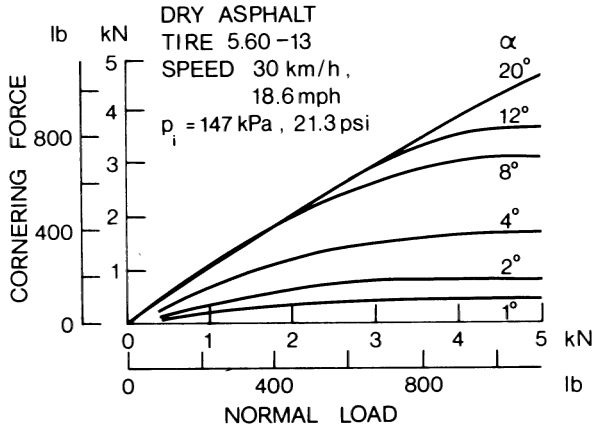


Fig. 1.25 Effect of normal load on the cornering characteristics of a car tire. (Reproduced with permission from *Mechanics of Pneumatic Tires*, edited by S.K. Clark, Monograph 122, National Bureau of Standards, 1971.)

state turn, owing to lateral load transfer, the normal load on the inside tire will be reduced to F_{zi} and that on the outside tire will be increased to F_{zo} . As a result, the total cornering force of the two tires will be the sum of F_{yi} and F_{yo} , which is less than $2F_y$, as shown in Fig. 1.26. This implies that for a pair of tires on a beam axle to develop the required amount of cornering force to balance a given centrifugal force during a turn, the lateral load transfer results in an increase in the slip angle of the tires.

To provide a measure for comparing the cornering behavior of different tires, a parameter called cornering stiffness C_α is used. It is defined as the derivative of the cornering force $F_{y\alpha}$ with respect to slip angle α evaluated at zero slip angle:

$$C_\alpha = \left. \frac{\partial F_{y\alpha}}{\partial \alpha} \right|_{\alpha=0} \quad (1.37)$$

Figure 1.27 shows a comparison of the relationships between the cornering

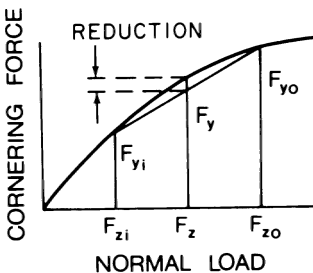


Fig. 1.26 Effect of lateral load transfer on the cornering capability of a pair of tires on an axle.

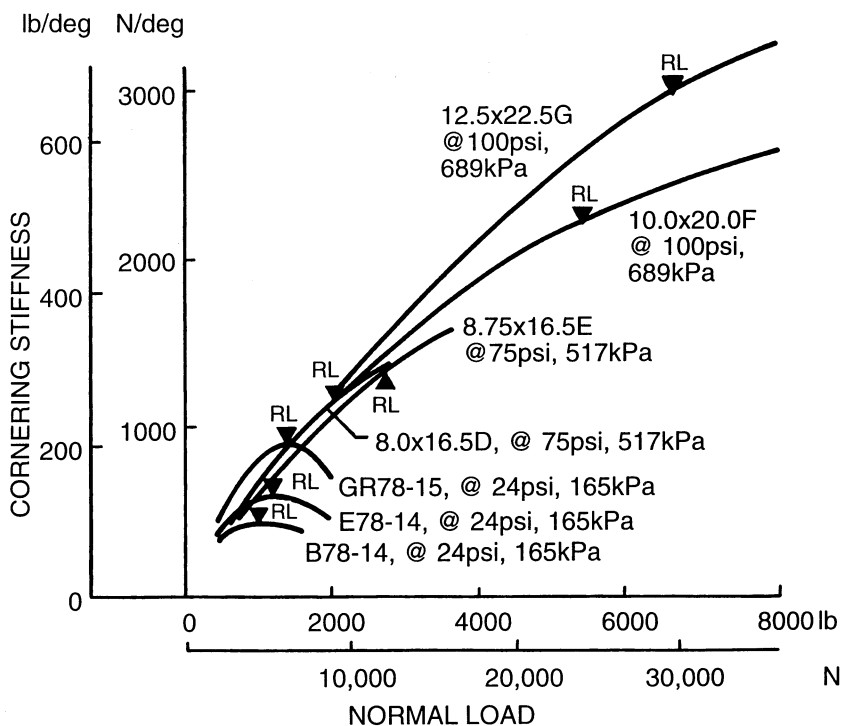


Fig. 1.27 Comparison of cornering stiffness of car, light truck, and heavy truck tires. (Reproduced with permission from reference 1.8.)

stiffness and the normal load for a sample of passenger car, light truck, and heavy truck tires [1.8]. In the figure, RL indicates the rated load for a specific tire. It can be seen that for the three passenger car tires tested, the cornering stiffness reaches a maximum at the rated load, and decreases with a further increase in the normal load. However, for the light truck and heavy truck tires shown, the cornering stiffness keeps increasing beyond the rated load, although at a lower rate.

To evaluate the effect of the normal load on the cornering ability of tires, a parameter called the cornering coefficient, which is defined as the cornering stiffness per unit normal load, is often used. Figure 1.28 shows a typical relationship between the cornering coefficient and the normal load of a tire [1.12]. It shows that the cornering coefficient decreases with an increase in the normal load.

Inflation pressure usually has a moderate effect on the cornering properties of a tire. In general, the cornering stiffness of tires increases with an increase of the inflation pressure. Figure 1.29 shows a comparison of the cornering coefficients at different inflation pressures of a radial-ply, a bias-belted, and a bias-ply passenger car tire [1.11]. Table 1.4 shows a sample of the values

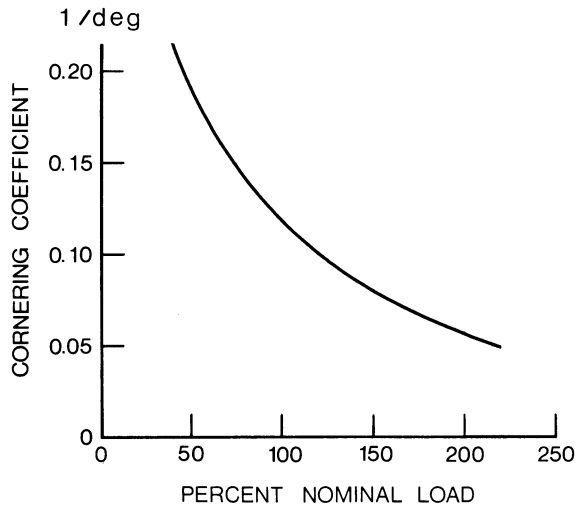


Fig. 1.28 Effect of normal load on the cornering coefficient of a tire. (Reproduced with permission from reference 1.12.)

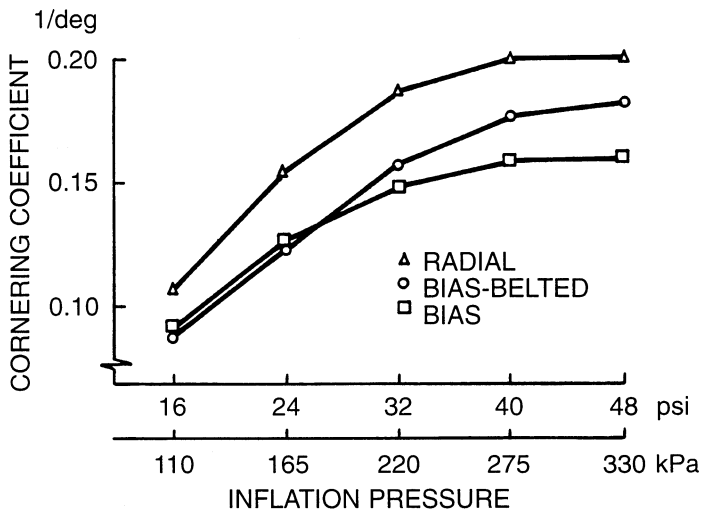


Fig. 1.29 Variation of cornering coefficient with inflation pressure for radial-ply, bias-ply, and bias-belted car tires. (Reproduced with permission of the Society of Automotive Engineers from reference 1.11.)

TABLE 1.4 Cornering Coefficients for Truck Tires at Rated Loads and Inflation Pressures (Unless Specified)

Tire Type	Tire Construction	Cornering Coefficient (deg^{-1})
Michelin Radial XZA (1/3 Tread)	Radial-ply	0.1861
Michelin Radial XZA (1/2 Tread)	Radial-ply	0.1749
Michelin Pilote XZA	Radial-ply	0.1648
Michelin Radial XZA	Radial-ply	0.1472
Goodyear Unisteel G159, 11R22.5 LRF at 655 kPa (95 psi)	Radial-ply	0.1413
Michelin XZZ	Radial-ply	0.1370
Goodyear Unisteel 11, 10R22.5 LRF at 620 kPa (90 psi)	Radial-ply	0.1350
Goodyear Unisteel G159, 11R22.5 LRG at 792 kPa (115 psi)	Radial-ply	0.1348
Goodyear Unisteel 11, 10R22.5 LRF at 758 kPa (110 psi)	Radial-ply	0.1311
Firestone Transteel	Radial-ply	0.1171
Firestone Transteel Traction	Radial-ply	0.1159
Goodyear Unisteel R-1	Radial-ply	0.1159
Goodyear Unisteel L-1	Radial-ply	0.1121
Firestone Transport 1	Bias-ply	0.1039
General GTX	Bias-ply	0.1017
Goodyear Super Hi Miler	Bias-ply	0.0956
Goodyear Custom Cross Rib	Bias-ply	0.0912
Uniroyal Fleet Master Super Lub	Bias-ply	0.0886
Firestone Transport 200	Bias-ply	0.0789

Source: UMTRI and TRIF, reference 1.19.

of the cornering coefficient for truck tires at rated loads and inflation pressures (unless specified) [1.19].

1.4.2 Slip Angle and Aligning Torque

As mentioned in Section 1.4.1, the side F_s applied at the wheel center and the cornering force $F_{y\alpha}$ developed in the ground plane are usually not collinear, as shown in Fig. 1.22. This gives rise to a torque commonly known as the aligning or self-aligning torque. Figure 1.30 shows a plot of the cornering force versus the aligning torque for a passenger car tire at various slip angles and under different normal loads [1.20]. Figure 1.31 and 1.32 show the variations of the aligning torque with the slip angle and the normal load for a bias-ply truck tire (10.00–20/ F) and for a radial-ply truck tire (10.00–20/ G), respectively [1.8]. It is interesting to note that with a given normal load, the aligning torque first increases with an increase of the slip angle. It reaches a maximum at a particular slip angle, and then decreases with a further increase